Journal of Hazardous Materials 171 (2009) 279–287

Contents lists available at ScienceDirect

Journal of Hazardous Materials

journal homepage: www.elsevier.com/locate/jhazmat

Controllable solvothermal synthesis and photocatalytic properties of complex (oxy)fluorides K_2TiOF_4, K_3TiOF_5, $K_7Ti_4O_4F_7$ and K_2TiF_6

Jie Sheng[a,b], Kaibin Tang[a,b,*], Wei Cheng[a,b], Junli Wang[a,b], Yanxiang Nie[a,b], Qing Yang[a,b]

[a] Division of Nanomaterials and Nanochemistry, Hefei National Laboratory for Physical Sciences at Microscale, Hefei, Anhui 230026, PR China
[b] Department of Chemistry, University of Science and Technology of China, Hefei, Anhui 230026, PR China

ARTICLE INFO

Article history:
Received 14 February 2009
Received in revised form 1 May 2009
Accepted 31 May 2009
Available online 7 June 2009

Keywords:
(Oxy)fluorides
Chemical synthesis
X-ray diffraction
Infrared spectroscopy
Photocatalytic properties

ABSTRACT

Complex (oxy)fluorides K_2TiF_6, K_2TiOF_4, K_3TiOF_5 and $K_7Ti_4O_4F_7$ have been successfully synthesized for the first time through a controllable solvothermal route involving different solvents, for example, methanol, methanol–H_2O and methanol–H_2O_2. The as-prepared products were characterized by X-ray powder diffraction, N_2 surface area adsorption, scanning electron microscope, Fourier transform infrared spectroscopy, UV–vis absorption spectra and X-ray fluorescence. The influences of reaction conditions such as the ratio of methanol to H_2O_2 or methanol to H_2O, reaction temperature on the phase, crystallizability and purity of the (oxy)fluorides products were discussed in detail. Meanwhile, the photocatalytic behaviors of the as-prepared K_2TiF_6, K_2TiOF_4, K_3TiOF_5 and $K_7Ti_4O_4F_7$ were evaluated by degradation of rhodamine B molecules, and the results showed that all of the products possessed photocatalytic activities in the order of $K_2TiOF_4 > K_2TiF_6 > K_7Ti_4O_4F_7 > K_3TiOF_5$ at room temperature under the UV light.

1. Introduction

Various new materials for photocatalysis have been synthesized in the past few decades [1–3]. A successful example is TiO_2, a metal oxide often used as a catalyst in photochemistry, electrochemistry, environmental protection, and in the battery industry [4,5]. Recently, F^- anion acting as promising dopant in a TiO_2 has attracted a great deal of attention [6–8]. F-doped TiO_2 samples showed stronger absorption in the UV-vis range and their photocatalytic activity exceeded that of Degussa P25 [9]. The interpretation of enhanced photocatalytic activities was as follows: (1) fluoride doping improves the crystallinity of oxides [6]; (2) the doped F atoms convert Ti^{4+} to Ti^{3+} and the presence of a certain amount of Ti^{3+} reduces the electron–hole recombination rate [7]; (3) fluorine doping results in the formation of oxygen vacancies and an increase of effective electron mobility [8]. In other words, effects of F^- doping on the structure, electronic chemistry and the transfer rate of photogenerated electrons to the photocatalyst surface are beneficial to an increase of photocatalytic activities [10]. It is well known that the studies of synthetic, structural, and electronic aspects of F^- for O^{2-} substitutions have also been particularly important [11,12]. For example, the synthesis of superconductor $Sr_2CuOF_{2+\delta}$ was reported [13]. That study showed that fluorine displaced oxide ions and caused a structural rearrangement to give a superconducting phase. In this oxyfluoride, the fluoride ion plays a dominant structural role rather than being merely an electronic dopant as in $La_2CuO_4F_x$ [14]. Therefore, the conclusion that the substitution of F^- for O^{2-} in structure is favorable to improve superconductivity may be a kind of useful enlightenment. It provides us a new way to reconsider the fluorine-containing photocatalysts, and thereby it also arouses our interest to explore photocatalytic performance of fluorides and oxyfluorides.

The Ti-based metal oxides (e.g. $SrTiO_3$, $K_2Ti_6O_{13}$ and $Na_2Ti_6O_{13}$) [15–17] have long been studied as UV light-responsive photocatalysts, this is mainly because of their favorable properties such as non-toxicity, chemical inertness, and high stability under light irradiation. However, little has been reported about the Ti-based metal fluoride and oxyfluoride materials as photocatalysts. Potassium fluorotitanate (K_2TiF_6) and potassium oxofluorotitanates (K_3TiOF_5, K_2TiOF_4 and $K_7Ti_4O_4F_7$) as complex (oxy)fluorides have been prepared using solid-state method or thermal decomposition route [18–21], but until now few studies have been conducted to uncover the properties of these compounds, besides the limit application of K_2TiF_6 such as additive [22] or reactant [23]. In this paper, we investigated the photocatalytic activity of these (oxy)fluorides utilizing the degradation of rhodamine B (RhB) aqueous solution under UV–vis light irradiation. Preliminary experiments showed that these complex materials possess different bandgaps for light energy conversion and displayed different photocatalytic activities.

In addition, we have also focused on the synthesis of (oxy)fluorides. Many different synthesis techniques have been used for preparation all kinds of (oxy)fluorides [24–30]. Direct syn-

* Corresponding author at: Division of Nanomaterials and Nanochemistry, Hefei National Laboratory for Physical Sciences at Microscale, Hefei, Anhui 230026, PR China. Tel.: +86 551 3601791.
E-mail address: kbtang@ustc.edu.cn (K. Tang).

0304-3894/$ – see front matter © 2009 Elsevier B.V. All rights reserved.
doi:10.1016/j.jhazmat.2009.05.141

thesis of these materials via simple route has attracted intensive interest in material science [31]. The mildly hydrothermal route as a typical solution approach has been proved to be effective and convenient in synthesizing various materials, for example, (oxy)fluoride functional materials [32–34] and (oxy)fluoride materials with open-framework [35]. The solvothermal approach is an evolution of hydrothermal synthesis, and it is also proved to be a facile and environmental friendly way. The required solvent can be used in the special systems to avoid the emergence of water and satisfy specific conditions. However, there are few reports about the solvothermal synthesis of oxyfluorides [36]. In the present case, we explored the feasibility of preparing the (oxy)fluorides K_2TiF_6, K_3TiOF_5, K_2TiOF_4 and $K_7Ti_4O_4F_7$ by employing a convenient solvothermal method at relatively low temperature.

2. Experimental

2.1. Preparation of the samples

Solvothermal synthesis of samples K_2TiF_6, K_3TiOF_5, K_2TiOF_4 and $K_7Ti_4O_4F_7$ was carried out in a Teflon-lined stainless steel autoclave under autogenously pressure. All the reagents (KOH, KF·$2H_2O$, TiO_2, Ti, NH_4HF_2, H_2O_2 and methanol) were purchased from Shanghai Chemical Reagent Company, and they were all analytically pure and used without further purification. The doses of starting materials for the synthesis of K_2TiF_6, K_2TiOF_4, K_3TiOF_5 and $K_7Ti_4O_4F_7$ were listed in Table 1. The mixture was put into a 50-mL Teflon-lined stainless autoclave which was then filled with methanol, methanol–H_2O or methanol–H_2O_2 up to 80% of the total volume. The autoclave was sealed quickly and heated at 200 °C for 24 h or 36 h, and then cooled to room temperature naturally. The precipitates were collected and washed with absolute ethanol, distilled water, respectively, and dried in vacuum at 60 °C for 2 h.

2.2. Sample characterizations

The samples were identified by X-ray powder diffraction (XRD) on a Philips X'pert PRO SUPER diffractometer with Cu-Kα radiation (λ = 1.541874 Å) at room temperature (40 kV, 30 mA) in the angular range of $10° < 2\theta < 70°$. The quantitative analysis of the products was carried out by XRF-1800 Sequential X-ray fluorescence spectrometer (XRF); the Fourier transform infrared spectra (FT-IR) were performed on a Magana IR-750 Ft spectrometer. The powders were dispersed in KBr (1.5/150 mg) and were studied at room temperature. UV–vis diffuse reflectance spectra (DRS) of the samples were measured by using Hitachi U-3010 UV–vis spectrophotometer. The scanning electron microscopy (SEM) images were taken on a Sirion 200 field emission scanning electron microscope (FE-SEM, 20 kV). The Brunauer–Emmett–Teller (BET) tests were determined via a Micromeritics ASAP-2000 nitrogen adsorption apparatus.

2.3. Photocatalytic test

Photocatalytic activities of the as-obtained samples were evaluated by the degradation of RhB under ultraviolet light irradiation of a 250 W Hg lamp and visible light irradiation of a 500 W Xe lamp. In each experiment, 100.0 mg sample as photocatalyst was added into 50 mL RhB solution (1.0×10^{-5} mol/L), and dispersed in an ultrasonic bath for 5 min. The solution was stirred for 10 min in the dark to reach adsorption equilibrium between catalyst and solution, and then was exposed to photo-irradiation. Concentrations of RhB were measured using UV–vis spectra (Shimadzu UV2550) every 5 min or longer time. Comparative experiments were also carried out with commercial Degussa P25 and without any photocatalysts on the same conditions.

3. Result and discussion

3.1. The fluoride K_2TiF_6 and the oxyfluoride K_2TiOF_4

3.1.1. Structure characterization

Fig. 1a shows the XRD pattern for the as-obtained Sample 1 (in Table 1). All of the diffraction peaks can be indexed as a hexagonal unit cell ($P\bar{3}m1$) with lattice parameters $a = 5.737$ Å, $c = 4.669$ Å, which were in good agreement with the reported data for K_2TiF_6 [JCPDS Card No. 08-0488: $a = 5.727$ Å, $c = 4.661$ Å]. No other characteristic peaks were observed for impurities, such as Ti, TiO_2, etc. Fig. 1b shows the XRD pattern of the as-prepared Sample 2. The diffraction peaks can be well indexed as the tetragonal K_2TiOF_4 with the lattice constants $a = 7.713$ Å, $c = 11.568$ Å (JCPDS Card No. 38-0984) and no peaks of impurities were detected. Furthermore, elementary analysis by XRF indicates that the molar ratios of K:Ti:F for Samples 1 and 2 are 1.88:1:5.85 and 1.74:1:3.84, respectively, which are close to the stoichiometry of K_2TiF_6 and K_2TiOF_4. SEM images of the as-prepared K_2TiF_6 and K_2TiOF_4 samples are shown in Fig. 2a and b, respectively. The K_2TiF_6 sample displays an irregular shape with the particle size less than 1 μm (Fig. 2a), and the sample K_2TiOF_4 also exhibits an irregular shape with an inhomogeneous particle size distribution (Fig. 2b). In order to illuminate the unhomogeneity, Scheme 1 gives a statistics graph to describe visually the particle size distribution of K_2TiOF_4, in which the particle size distribution collected mostly in a narrow region less than 2 μm.

3.1.2. Influences of reaction conditions on the products

In the work, the volume ratio of solvent CH_3OH/H_2O_2 and reaction temperature were found to play vital roles on the formation, crystallizability and purity of K_2TiF_6 and K_2TiOF_4 samples. They were investigated systematically, and the results are listed in Table 2. Ti, KOH and NH_4HF_2 as reactants and mineralizers were employed to prepare K_2TiF_6 and K_2TiOF_4 in the reaction [37]. The phase formation of K_2TiF_6 and K_2TiOF_4 could be easily accessed by controlling the volume ratio (CH_3OH/H_2O_2) and reaction temperature.

The pure and well-crystalline K_2TiF_6 sample was typically prepared at 200 °C for 24 h in an appropriate solvent composed of CH_3OH and H_2O_2 with volume ratio of 3:1 (No. 1 of Table 2). When the ratio of CH_3OH to H_2O_2 was altered to 4:1 or 2:1 without changing other conditions, it was found that K_2TiF_6 was the dominant phase and always coexisted with impurities in final products, e.g.

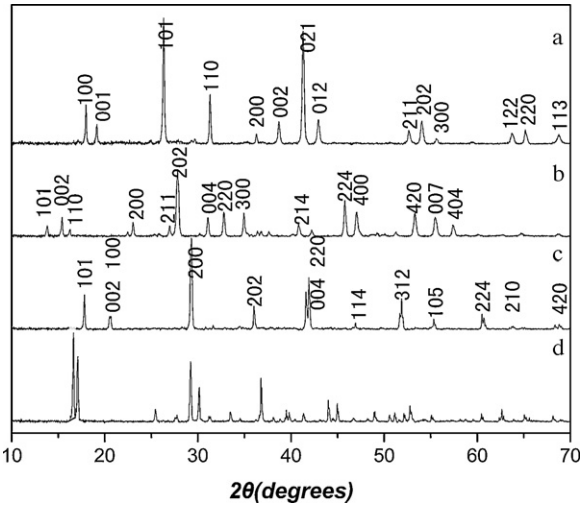

Fig. 1. The XRD patterns of the desired products obtained by solvothermal synthesis with feasible conditions (a) K_2TiF_6, (b) K_2TiOF_4, (c) K_3TiOF_5, and (d) $K_7Ti_4O_4F_7$.

Table 1
Feasible conditions for solvothermal synthesis of K_2TiF_6, K_2TiOF_4, K_3TiOF_5 and $K_7Ti_4O_4F_7$.

No.	Starting materials					Mole ratio	Temperature (°C)	Time (h)	Solvent (volume ratio)	Products
	a	b	c	d	e					
Sample 1	–	Ti	KOH	–	NH_4HF_2	1:2:3	200	24	CH_3OH:H_2O_2 (3:1)	K_2TiF_6
Sample 2	–	Ti	KOH	–	NH_4HF_2	1:2:2	200	24	CH_3OH:H_2O_2 (1:1)	K_2TiOF_4
Sample 3	TiO_2	–	–	KF	–	1:5.5	200	24	CH_3OH	K_3TiOF_5
Sample 4	TiO_2	–	KOH	KF	–	1:1:2	200	36	CH_3OH:H_2O (1:1)	$K_7Ti_4O_4F_7$

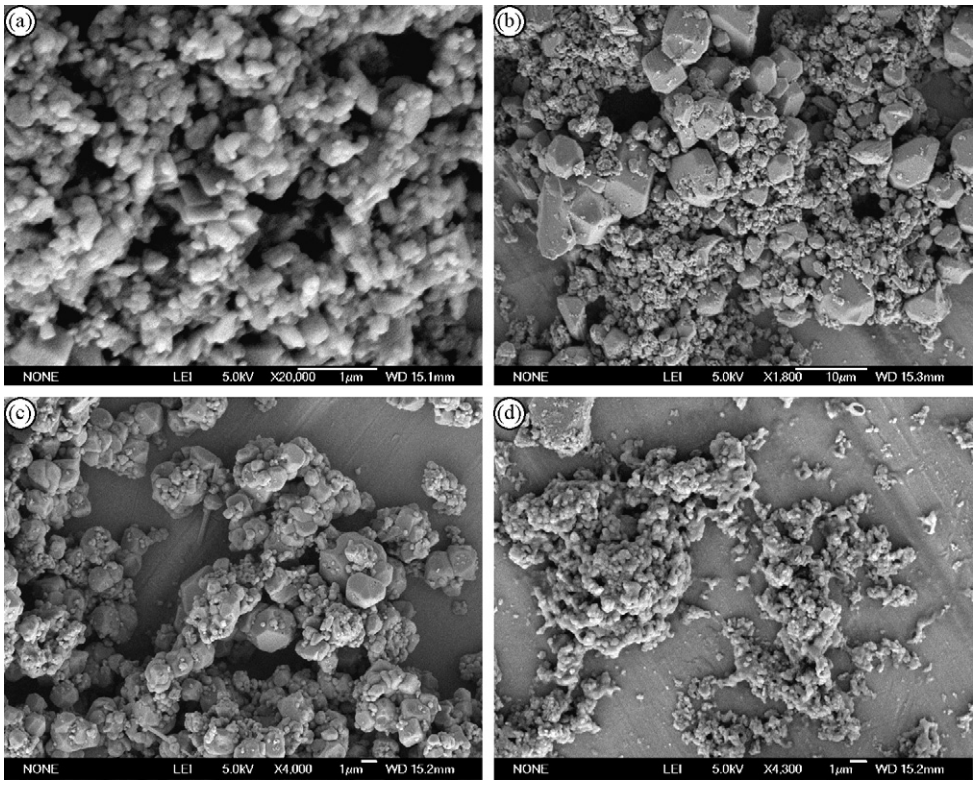

Fig. 2. SEM images of the as-obtained samples: (a) K_2TiF_6, (b) K_2TiOF_4, (c) K_3TiOF_5, and (d) $K_7Ti_4O_4F_7$.

TiO_2, $TiOF_2$ or hydrated oxyfluorides (Nos. 2 and 3). Table 2 also shows the effects of reaction temperature on the final products. When the reaction was carried out at 100 °C for 12 h or 48 h, K_2TiF_6 was always accompanied by byproducts in the final products (Nos. 4 and 5). When the reaction temperature increased to 250 °C, the desired K_2TiF_6 sample could be also obtained (No. 6).

The volume ratio of CH_3OH/H_2O_2 and temperature also greatly affected the synthesis of K_2TiOF_4. Typically, K_2TiOF_4 was successfully obtained when the synthesis was performed at 200 °C for 24 h with CH_3OH/H_2O_2 = 1:1 in volume ratio (No. 7). While the ratio descended to 0.5, the final products contained K_2TiOF_4 and a little impurity, e.g. TiO_2. In the experiments, we found that the phase-pure K_2TiOF_4 could be obtained at higher temperature (≥200 °C), while multiphase samples with impurities were produced at lower temperature (100 °C) (Nos. 8–10 in Table 2). Thus, the formation of K_2TiOF_4 and K_2TiF_6 was much sensitive to the ratio of solvents, which could be attributed to the competitive results between the O and F species. It is known that fluorine can substitute easily oxygen in solid-state chemistry due to the similar size of the O^{2-} and F^-. Usually, K_2TiOF_4 can be facilely acquired with volume ratio of

Table 2
Variant conditions for solvothermal synthesis of K_2TiF_6 and K_2TiOF_4.

No.	Starting material ratio			Solvent volume ratio		Temperature (°C)	Time (h)	Products
	Ti	KOH	NH_4HF_2	CH_3OH	H_2O_2			
1	1	2	3	3	1	200	24	K_2TiF_6
2	1	2	3	4	1	200	24	K_2TiF_6 + impurities
3	1	2	3	2	1	200	24	K_2TiF_6 + K_2TiOF_4 + impurities
4	1	2	3	3	1	100	48	K_2TiF_6 + impurities
5	1	2	3	3	1	100	12	K_2TiF_6 + impurities
6	1	2	3	3	1	250	12	K_2TiF_6
7	1	2	2	1	1	200	24	K_2TiOF_4
8	1	2	2	1	1	250	12	K_2TiOF_4
9	1	2	2	1	1	100	48	K_2TiOF_4 + impurities
10	1	2	2	1	1	100	12	K_2TiOF_4 + impurities
11	1	2	2	0.5	1	200	24	K_2TiOF_4 + impurities

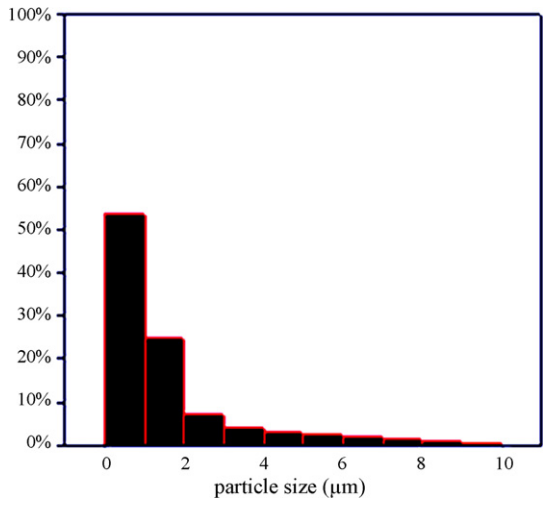

Scheme 1. Particle size distributions of Sample 2 (K_2TiOF_4).

1:1 (CH_3OH to H_2O_2), whereas, the decrease of H_2O_2 led to the increase of fluorine content relative to oxygen, and that fluorine took over competitive advantageous status in the reaction. Finally, the free-oxygen compound K_2TiF_6 was obtained.

3.2. The oxyfluoride K_3TiOF_5 and $K_7Ti_4O_4F_7$

3.2.1. Structure characterization

The powder X-ray diffraction pattern of Sample 3 (in Table 1) is shown in Fig. 1c. All of the diffraction peaks can be well indexed as the tetragonal K_3TiOF_5 (JCPDS Card No. 23-0506) with lattice parameters of $a = 6.102$ Å, $c = 8.655$ Å. No characteristic peaks of impurities were detected. Further investigation of XRF shows that the molar ratio of K:Ti:F for Sample 3 is 3.07:1:5.27 close to the stoichiometry of K_3TiOF_5, which confirmed the production of phase-pure K_3TiOF_5 sample. Fig. 1d shows the XRD pattern of Sample 4. The observed 2θ values and intensities of reflection lines were consistent with the reported values of $K_7Ti_4O_4F_7$ (JCPDS Card No. 420354), and it indicated that Sample 4 could be obtained with the nominal composition of $K_7Ti_4O_4F_7$. Similarly, the analysis of XRF was also carried out to further verify the composition of Sample 4. The result reveals that its molar ratio of K:Ti:F equal to 2.02:1:1.65, which roughly agrees with the stoichiometry of $K_7Ti_4O_4F_7$.

Fig. 2c shows SEM image of the as-obtained K_3TiOF_5 sample, which was composed of many microparticles and irregular polyhedra with 0.5–5 μm in diameter. SEM image of the as-synthesized $K_7Ti_4O_4F_7$ sample is shown in Fig. 2d, and it revealed that the sample was also comprised of irregular particles with around 0.5 μm in diameters and displayed a tendency of conglomeration.

3.2.2. Influences of reaction conditions on the products

The solvents and Ti-sources in the synthesis of K_3TiOF_5 and $K_7Ti_4O_4F_7$ were different from that of K_2TiF_6 and K_2TiOF_4. The detailed information is summarized in Table 3. The pure K_3TiOF_5 sample was successfully prepared using TiO_2 and $KF{\cdot}2H_2O$ as reaction reagents at 200 °C for 24 h in methanol solvent (No. 1 in Table 3). It was found that the reaction temperature was also an important factor to produce the K_3TiOF_5 sample, and the higher temperature was favorable for the formation of pure K_3TiOF_5. Whereas, when the synthesis was carried out at the lower temperature than 100 °C, no K_3TiOF_5 was obtained (Nos. 4 and 5) even though the reaction time increased to 48 h. When the temperature increased to 250 °C, the single phase K_3TiOF_5 could be obtained with the reaction time shortened to 12 h (No. 6). The dose of KOH had greatly impact on the final results in the reaction. If 0.1 mmol KOH was added, K_3TiOF_5 always appeared along with impurities; while 0.5 mmol KOH was employed in experiment, K_3TiOF_5 was scarcely obtained (Nos. 2 and 3).

The formation of $K_7Ti_4O_4F_7$ was also very sensitive to the preparative conditions such as CH_3OH/H_2O volume ratio, temperature and the basicity of solution. Typically, the pure $K_7Ti_4O_4F_7$ could be received at 200 °C for 36 h in the mixed solvent ($CH_3OH/H_2O = 1/1$ in volume ratio), using TiO_2, KOH and NH_4HF_2 as starting material. The effects of CH_3OH/H_2O on the formation of $K_7Ti_4O_4F_7$ are shown in Table 3. When the ratio (CH_3OH/H_2O) changed from 1/1 to 2/1, as-obtained $K_7Ti_4O_4F_7$ sample contained impure phases, e.g. TiO_2 (Nos. 7 and 8). Table 3 also reveals the influences of reaction temperature on the formation of $K_7Ti_4O_4F_7$, which was similar to that of K_3TiOF_5. No $K_7Ti_4O_4F_7$ was observed at lower temperature (100 °C), and it could be acquired at higher temperature (≥200 °C) under the similar conditions (Nos. 9 and 10). The excessive KOH would not favor for the production of pure $K_7Ti_4O_4F_7$ (Nos. 11 and 12), but TiO_2 dominated the final products in the high alkaline solution. The two synthetic strategies were similar to that of K_2TiF_6 and K_2TiOF_4, and that there also existed competition between fluorine and oxygen anions in the reactions. The use of anhydrous methanol resulted in competitive advantage of F^- to O^{2-} anions in the reaction system. Due to large proportion of fluorine content, it should be reasonable that K_3TiOF_5 rather than $K_7Ti_4O_4F_7$ with low fluorine content was obtained in anhydrous methanol. In contrary, $K_7Ti_4O_4F_7$ instead of K_3TiOF_5 could emerge in the reaction using the mixed solvent of CH_3OH and H_2O.

3.3. FT-IR analysis

In order to further demonstrate the character of as-prepared (oxy)fluorides, the FT-IR spectra of the products are presented in Fig. 3, in which all samples exhibit main absorption bands at 450–1000 cm^{-1}. Fig. 3a shows the characteristic absorption peak of the as-prepared K_2TiF_6 products, which is loaded at 579 cm^{-1}, consistent with the reported values of absorption band of TiF_6^{2-} in K_2TiF_6 [38]. The absorption peaks of the as-prepared K_2TiOF_4 sample are present at 530 cm^{-1} and 873 cm^{-1} (shown in Fig. 3b), which can be ascribed to the stretching vibration of Ti–F and Ti–O (terminal oxygen), respectively. Moreover, the absorption bands overlapped with others at 466 cm^{-1} and 828 cm^{-1} (indicated with arrows in Fig. 3b) probably resulted from fluorine and terminal oxygen presenting and distributed in the crystal lattice randomly [39]. The FT-IR spectrum of obtained K_3TiOF_5 sample is shown in Fig. 3c, and the strong absorption peaks at 514 cm^{-1} and 896 cm^{-1} are ascribed to the stretching vibration of Ti–F and Ti–O (terminal oxygen) of K_3TiOF_5, respectively. Fig. 3d displays the IR spectrum of the as-prepared $K_7Ti_4O_4F_7$ products. The peak at 554 cm^{-1} can be assigned to the stretching vibration of Ti–F, and the peaks at 1100–750 cm^{-1} could be attributed to the presence of Ti–O bond or to a combination lattice mode of Ti–O and Ti–F bands in $K_7Ti_4O_4F_7$ [39]. It is noted that in all the IR spectra (4000–1100 cm^{-1}) of the four samples, no peaks of impurities were detected except for two broad absorption bands around 3450 cm^{-1} (O–H stretching) and 1630 cm^{-1} (H–O–H bending), which were due to water molecules absorbed from air. The results suggest that all samples have not been incorporated with N, C species, which confirms the absence of NH_4^+ or absorbed organic molecules in the (oxy)fluorides products. It is found that no Ti–O characteristic absorption peaks (750–900 cm^{-1}) were observed in Fig. 3a, indicating that no –OH or oxygen binding to Ti in crystal lattice of as-prepared K_2TiF_6. Because of almost identical shapes and relative intensity of absorption peaks from water molecules in all FT-IR spectra (Fig. 3) of the obtained (oxy)fluorides samples, it is clear that there are no OH groups taking up the position of crystal lattice of all the prepared (oxy)fluorides.

Table 3
Variant conditions for solvothermal synthesis of K_3TiOF_5 and $K_7Ti_4O_4F_7$.

No.	Starting materials ratio			Solvent volume (ml)		Temperature (°C)	Time (h)	Products
	TiO_2	KOH	KF	CH_3OH	H_2O			
1	1	–	5.5	40	–	200	24	K_3TiOF_5
2	1	–	5.5	40	–	100	24	TiO_2 + impurities
3	1	–	5.5	40	–	100	48	TiO_2 + impurities
4	1	–	5.5	40	–	250	12	K_3TiOF_5
5	1	0.1	5.5	40	–	200	48	K_3TiOF_5 + impurities
6	1	0.5	5.5	40	–	200	12	multiphase
7	1	1	2	20	20	200	36	$K_7Ti_4O_4F_7$
8	1	1	2	30	15	200	36	$K_7Ti_4O_4F_7$ + impurities
9	1	1	2	20	20	100	36	TiO_2 + impurities
10	1	1	2	20	20	250	20	$K_7Ti_4O_4F_7$
11	1	3	2	20	20	200	36	$K_7Ti_4O_4F_7$ + impurities
12	1	4	2	20	20	200	36	TiO_2 + impurities

3.4. Photoabsorption properties

Photoabsorption ability of the (oxy)fluorides was detected by UV–vis diffuse reflectance spectra, as shown in Fig. 4. The sample K_2TiF_6 presented the photoabsorption properties from the UV-light to visible light region shorter than 450 nm (Fig. 4a). The steep shape of spectrum indicated that the visible-light absorption was due to the bandgap transition of K_2TiF_6, but the transition from the impurity. For a crystalline semiconductor, it was known that the optical absorption near the band edge followed the equation $(\alpha h\nu)^n = A(h\nu - E_g)$, where α, ν, E_g, and A were absorption coefficient, light frequency, bandgap, and constant, respectively, while the value of n is decided by the characteristics of transition in a semiconductor. According to the equation, the bandgap (E_g) of K_2TiF_6 was estimated to be 3.44 eV (direct transition) from the onset of absorption edge (inset in Fig. 4a). Similarly, the optical absorption properties of K_2TiOF_4, K_3TiOF_5 and $K_7Ti_4O_4F_7$ were revealed in Fig. 4b–d, and the values of E_g of three samples corresponding to direct transition were determined to be 3.21 eV, 3.94 eV and 4.39 eV, respectively. Fig. 4b shows that K_2TiOF_4 possesses a broad absorption band appeared in the range of 350–670 nm, and a minimum bandgap compared with those of other three samples. It is known that the mechanism of photocatalytic reactivity is the result of multiple effects from bandgap energy (E_g), photoproduced hole–electron separation and the charge transport, energy levels of valence band and conduce band, surface areas of materials and so on. In the work, the catalytic mechanism was not explained detailedly, but the bandgap energies determined by the absorption spectra have been presented, which indicate that these (oxy)fluorides were the wide-bandgap semiconductors and they may become potential photocatalysts.

3.5. BET surface areas of K_2TiF_6, K_2TiOF_4, K_3TiOF_5 and $K_7Ti_4O_4F_7$

Fig. 5a–d represents the nitrogen adsorption–desorption isotherms and BJH pore size distribution curves (inset) of the (oxy)fluorides K_2TiF_6, K_2TiOF_4, K_3TiOF_5 and $K_7Ti_4O_4F_7$ by solvothermal route, respectively. The typical isotherms were identified as type II with the hysteresis loop of H3 type suggest that

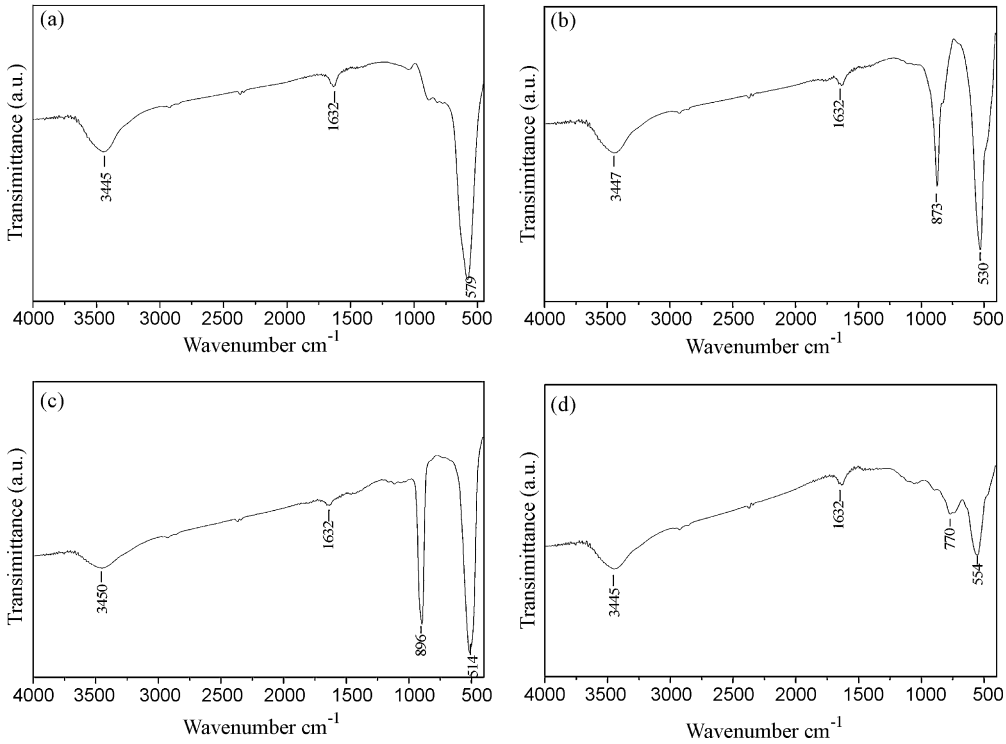

Fig. 3. FT-IR spectra of the as-obtained samples: (a) K_2TiF_6, (b) K_2TiOF_4, (c) K_3TiOF_5, and (d) $K_7Ti_4O_4F_7$.

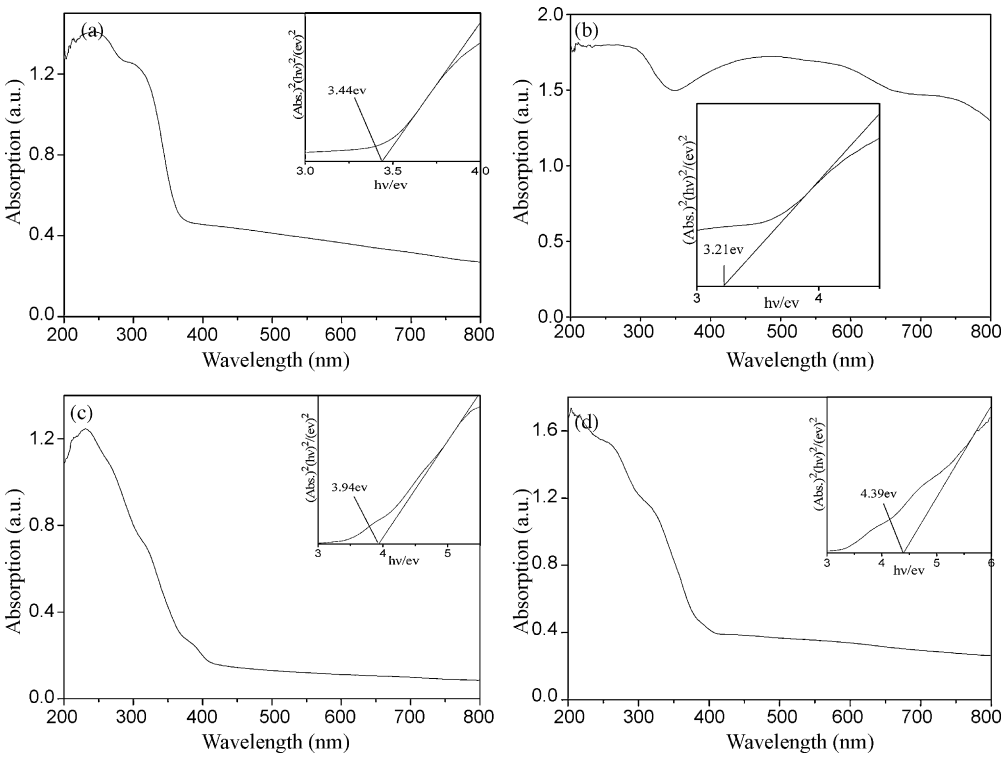

Fig. 4. UV–vis diffuse reflectance spectra of as-obtained samples: (a) K_2TiF_6, (b) K_2TiOF_4, (c) K_3TiOF_5, and (d) $K_7Ti_4O_4F_7$. The insets shows the bandgap (E_g) of these (oxy)fluorides, which were estimated to be 3.44 eV, 3.21 eV, 3.94 eV and 4.39 eV from the onset of the absorption edge, respectively.

all products possessed characteristic structures with nonporous or macroporous adsorbents and unrestricted monolayer–multilayer adsorption [40]. Table 4 summarizes the surface area (S_{BET}), pore volume (V_P), and pore diameter (D_p) of different products calculated by the BJH method based on the nitrogen adsorption–desorption isotherms. The surface areas of K_2TiF_6, K_2TiOF_4, K_3TiOF_5 and $K_7Ti_4O_4F_7$ are 5.4696, 1.4367, 2.5253 and 3.9880 m^2/g, respectively, all of which are much smaller than that of the Degussa P25

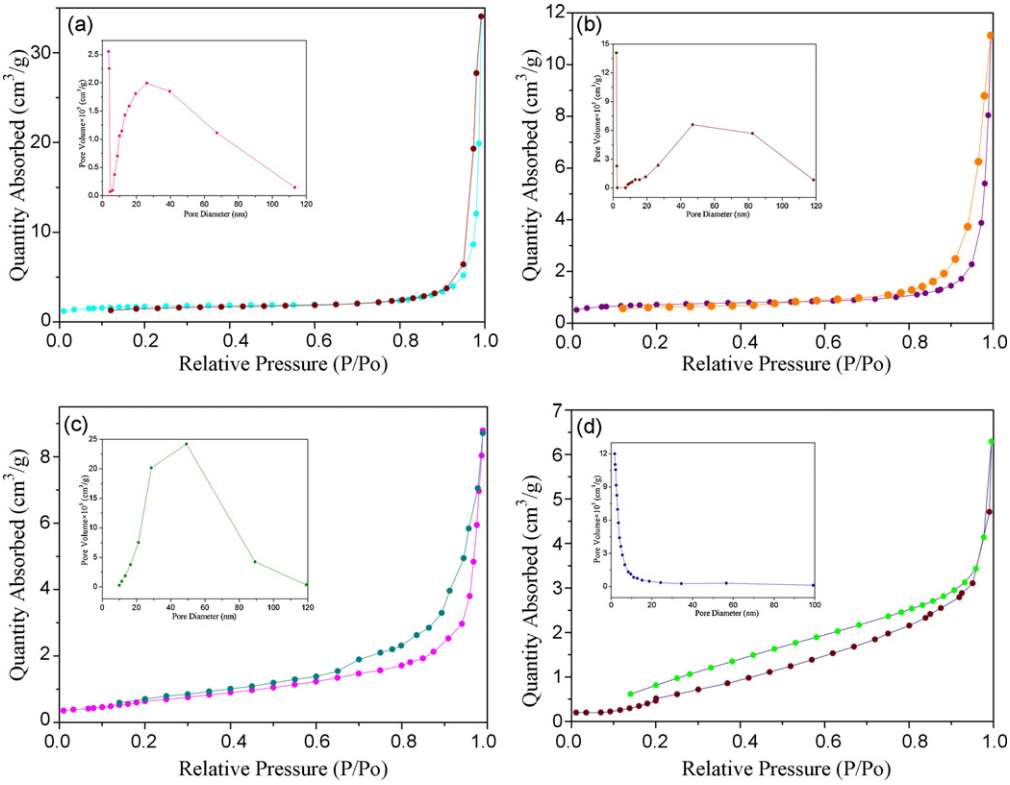

Fig. 5. Nitrogen adsorption–desorption isotherms of as-obtained samples: (a) K_2TiF_6, (b) K_2TiOF_4, (c) K_3TiOF_5, and (d) $K_7Ti_4O_4F_7$. The insets show their BJH pore size, respectively.

Table 4
Textural properties of K_2TiF_6, K_2TiOF_4, K_3TiOF_5 and $K_7Ti_4O_4F_7$.

Sample	A_{BET} (m^2/g)	D_P (nm)	V_P (cm^3/g)
K_2TiF_6	5.4696	38.5	0.053
K_2TiOF_4	1.4367	22.0	0.0065
K_3TiOF_5	2.5253	9.8	0.0098
$K_7Ti_4O_4F_7$	3.9880	30.5	0.017
P25	50	–	–

TiO_2 (50 m^2/g) from the linear part of the BET plots. The average pore size for these (oxy)fluorides are about 38.5, 22.0, 9.8 and 30.5 nm, respectively, with nonuniform distribution of pore size, and their pore volume are about 0.053, 0.0065, 0.0098 and 0.017 cm^3/g, respectively. The pores originating from the interparticles space are very lower, which can be shown in the SEM image (Fig. 2).

3.6. Photocatalytic activities

It is well known that light absorption of materials and the migration of the light-induced electrons and holes are key factors controlling a photocatalytic reaction, which are relevant to the electronic structure characteristics of materials [41–43]. The absorption spectra (in Fig. 4) display that the (oxy)fluorides possess intense absorption in the UV–vis light regions, which means as-prepared (oxy)fluorides could be regarded as candidate photocatalysts. The photocatalytic efficiency of the samples was evaluated by degrading RhB solution. Fig. 6 displays the temporal evolution of the relative RhB concentration during the photodegradation mediated by K_2TiF_6, K_2TiOF_4, K_3TiOF_5 and $K_7Ti_4O_4F_7$ under UV light illumination, which exhibited clearly that all samples possessed fine photocatalytic properties for the degradation of RhB. By comparison, it can be observed that their catalytic efficiency was as follows: $K_2TiOF_4 > K_2TiF_6 > K_7Ti_4O_4F_7 > K_3TiOF_5$. Especially, K_2TiOF_4 with the highest activity was almost comparable to the Degussa P25 sample under UV light irradiation. In addition, a blank test has been performed without photocatalyst under UV light illumination, which demonstrated that the degradation of RhB was extremely slow. The result of the commercial Degussa P25 on the same conditions shows that degradation percentage of RhB solution was up to 96% within 20 min of irradiation. It is know that the BET surface areas are closely related to the photocatalytic activities, in another word, the high BET surface areas are mainly factor contributing to the high photocatalytic activities for many photocatalysts [44]. However, the BET surface areas of these

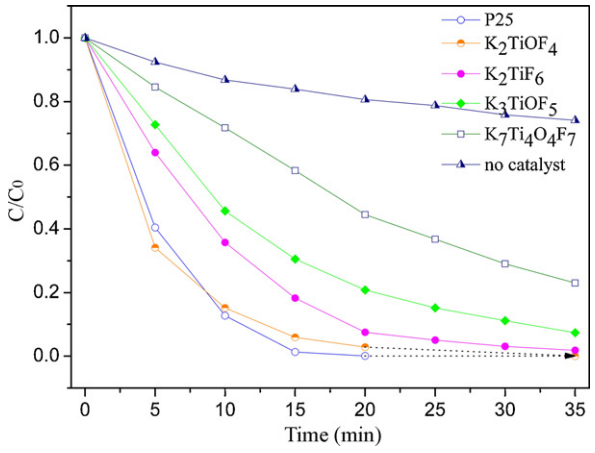

Fig. 6. Comparison of photocatalytic activity for different photocatalysts by decomposing rhodamine B (RhB) under UV-light irradiation.

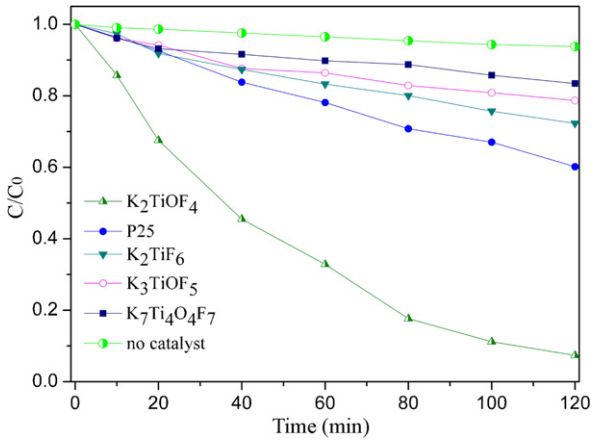

Fig. 7. Comparison of photocatalytic activity for different photocatalysts by decomposing rhodamine B (RhB) under visible-light irradiation.

(oxy)fluorides (<10 m^2/g) were much small comparing with the P25 (50 m^2/g). Therefore, the possible reasons inducing high photocatalytic activities should be attributed to their self-structure feature. In addition, the photocatalytic activity of K_2TiOF_4 was the highest among that of these (oxy)fluorides, which was almost comparable to that of the commercial Degussa P25, but K_2TiOF_4 possessed with the narrowest bandgap (E_g = 3.21 eV). The relationship between catalytic activity and E_g of the catalysts is not clear, and the specific photocatalytic mechanism needed to be further explored.

It should be noted that K_2TiOF_4 shows an intense photoabsorption in the visible light region ($\lambda > 420$ nm, see Fig. 4b). This means that the compound can utilize more irradiation light energy and has also the ability to respond to the wavelength of visible light region. In order to further explore photocatalytic performance, The RhB decomposition catalyzed by K_2TiF_6, K_3TiOF_5 and $K_7Ti_4O_4F_7$ was investigated under visible light irradiation ($\lambda > 420$ nm). As a comparison, the RhB photodegraded by Degussa P25 was also performed. The blank experiment without the photocatalyst was investigated under the same conditions. The RhB concentrations versus the reaction time in these (oxy)fluorides and P25 systems as well as the blank experiment are plotted in Fig. 7, respectively. It can be clearly seen that the K_2TiF_6, K_3TiOF_5 and $K_7Ti_4O_4F_7$ (oxy)fluorides exhibit extremely slow degradation ratio under visible light irradiation. The commercial Degussa P25 was obviously inactive under visible light irradiation, as reported by Asahi et al. [45]. RhB photolysis without the photocatalyst could almost be neglected in identical conditions. However, the photocatalytic activity of K_2TiOF_4 was the most significant under visible light irradiation, the degradation ratio of RhB was up to 93% after 120 min of irradiation. It is not surprising, Liu et al. [46] have also synthesized two doped photocatalysts $Cs_{0.68}Ti_{1.83}O_{4-x}N_x$ and $H_{0.68}Ti_{1.83}O_{4-x}N_x$, which have an extraordinary band-to-band shift from 356 and 380 nm to 472 and 453 nm Comparing with $Cs_{0.68}Ti_{1.83}O_4$, $H_{0.68}Ti_{1.83}O_4$, respectively, and that the photocatalysts do better work under visible light irradiation. An efficient doping strategy could lead to the photoabsorption occurring in visible light region, the bandgap energy decreasing distinctly, and the visible-light-driven photoactivity enhancing greatly. Commonly, an efficient photocatalytic process is subject to the direct absorption of a photon by the energy bandgap of the materials. Huang [47] has prepared oxhalide BiOCl, which possesses an open (loose packed) structure and an indirect-transitions bandgap. This may benefit the hole–electron separation and the charge transport. The high photocatalytic activity of K_2TiOF_4 can only be achieved under visible light in our case,

the energy level and the unique band structure of the K_2TiOF_4 may play a crucial role in determining its photocatalytic activity. Further research is under way to achieve a full understanding of this novel photocatalyst.

4. Conclusions

In summary, the controllable synthesis of the complex (oxy)fluorides K_2TiOF_4, K_3TiOF_5, $K_7Ti_4O_4F_7$ and K_2TiF_6 was successfully realized via a mild solvothermal route at 200 °C for the first time, which was proved by a variety of characterizations including XRD, FT-IR, and XRF. Investigations showed that the components of solvents and their volume ratio were important factors in the formation of these (oxy)fluorides. In this paper, our results revealed that there were optimum CH_3OH/H_2O_2 volume ratio for the formation of K_2TiF_6 and K_2TiOF_4. The anhydrous methanol was in favor of preparing the pure K_3TiOF_5, however, $K_7Ti_4O_4F_7$ could be obtained using the mixture of CH_3OH and H_2O (volume ratio 1:1) as solvent at identical reaction conditions. Furthermore, the reaction temperature was also a principal factor affecting the formation of the products, which was beneficial to synthesis of these (oxy)fluorides above 200 °C. UV–vis absorption spectra indicated all products possessed larger bandgap from direct transition. Despite of the lower BET surface area, the as-prepared K_2TiOF_4, K_3TiOF_5, $K_7Ti_4O_4F_7$ and K_2TiF_6 still displayed good photocatalytic performances for the degradation of RhB aqueous solution under UV light irradiation with a activity sequence as following: $K_2TiOF_4 > K_2TiF_6 > K_7Ti_4O_4F_7 > K_3TiOF_5$. In particular, the photocatalytic activity of K_2TiOF_4 was comparable to that of the commercial Degussa P25 for UV light, moreover, K_2TiOF_4 also showed high visible-light photocatalytic activity in degrading RhB. All these indicate that the as-prepared complex (oxy)fluorides were novel and active photocatalysts which may find potential application in photocatalytic fields in the future.

Acknowledgments

Financial supports by the National Natural Science Foundation of China (No. 20371044, 20621061), the 973 Projects of China and the Program for New Century Excellent Talents in university (NCET) are gratefully acknowledged.

References

[1] M.R. Hoffmann, S.T. Martin, W. Choi, D.W. Bahnemann, Environmental applications of semiconductor photocatalysis, Chem. Rev. 95 (1995) 69–96.
[2] M. Anpo, M. Takeuchi, The design and development of highly reactive titanium oxide photocatalysts operating under visible light irradiation, J. Catal. 216 (2003) 505–516.
[3] A. Fihri, V. Artero, M. Razavet, C. Baffert, W. Leibl, M. Fontecave, Cobaloxime-based photocatalytic devices for hydrogen production, Angew. Chem. Int. Ed. 47 (2008) 564–567.
[4] I. Salem, Recent studies on the catalytic activity of titanium, zirconium, and hafnium oxides, Catal. Rev. Sci. Eng. 45 (2003) 205–296.
[5] A.L. Linsebigler, G. Lu, J.T. Yates, Photocatalysis on TiO_2 surfaces: principles, mechanisms, and selected results, Chem. Rev. 95 (1995) 735–758.
[6] A. Hattori, H. Tada, High photocatalytic activity of F-doped TiO_2 film on glass, J. Sol-Gel Sci. Technol. 22 (2001) 47–52.
[7] J.C. Yu, J.G. Yu, W. Ho, Z. Jiang, L. Zhang, Effects of F-doping on the photocatalytic activity and microstructures of nanocrystalline TiO_2 powders, Chem. Mater. 14 (2002) 3808–3816.
[8] J.S. Wang, S. Yin, Q.W. Zhang, F. Saito, T. Sato, Mechanochemical synthesis of $SrTiO_{3-x}F_x$ with high visible light photocatalytic activities for nitrogen monoxide destruction, J. Mater. Chem. 13 (2003) 2348–2352.
[9] J.C. Yu, J. Yu, W. Ho, Z. Jiang, L. Zhang, Effects of F-doping on the photocatalytic activity and microstructures of nanocrystalline TiO_2 powders, Chem. Mater. 14 (2002) 3808–3816.
[10] G.L. Huang, Y.F. Zhu, Enhanced photocatalytic activity of $ZnWO_4$ catalyst via fluorine doping, J. Phys. Chem. C 111 (2007) 11952–11958.
[11] M. Al-Mamouri, P.P. Edwards, C. Greaves, M. Slaski, Synthesis and superconducting properties of the strontium copper oxy-fluoride $Sr_2CuO_2F_{2+\delta}$, Nature. 369 (1994) 382–384.
[12] A.M. Abakumov, M.G. Rozova, E.I. Ardashnikova, E.V. Antipov, High-temperature superconductors based on complex layered copper oxyfluorides, Russ. Chem. Rev. 71 (2002) 383–399.
[13] M.G. Francesconi, P.R. Slater, J.P. Hodges, C. Greaves, P.P. Edwards, M. Al-Mamouri, M. Slaski, Superconducting $Sr_{2-x}A_xCuO_2F_{2+\delta}$ (A = Ca, Ba): synthetic pathways and associated structural rearrangements, J. Solid State Chem. 135 (1998) 17–27.
[14] B.M. Tissue, K.M. Cirillo, J.C. Wright, M. Daeumling, D.C. Larbalestier, Conversion of $La_2CuO_{4-\delta}$ to a superconductor by treatment in fluorine gas, Solid State Commun. 65 (1988) 51–54.
[15] J.S. Wang, S. Yin, T. Sato, Synthesis and characterization of fibrous $SrTiO_3$ particles, Mater. Sci. Eng. B 131 (2006) 248–251.
[16] G. Guan, T. Kida, T. Harada, M. Isayama, A. Yoshida, Photoreduction of carbon dioxide with water over $K_2Ti_6O_{13}$ photocatalyst combined with Cu/ZnO catalyst under concentrated sunlight, Appl. Catal. A: Gen. 249 (2003) 11–18.
[17] M. Kohno, S. Ogura, K. Sato, Y. Inoue, Effect of tunnel structures of $BaTi_4O_9$ and $Na_2Ti_6O_{13}$ on photocatalytic activity and photoexcited charge separation, Stud. Surf. Sci. Catal. 101 (1996) 143–152.
[18] P.M. Perillo, O. Ares, J. Botbol, Potassium flurotitanate preparation, Ann. Chim.-Sci. Mater. 17 (1992) 261–267.
[19] G. Pausewang, W. Rudorff, Über Alkali-oxofluorometallate der Übergangsmetalle $A_3^IMeO_xF_{6-x}$-Verbindungen mit $x = 1, 2, 3$, Z. Anorg. Allg. Chem. 364 (1969) 69–87.
[20] G. Pausewang, R.S. Tubingen, Zur Existenz der Verbindung K_2TiOF_4: Pyrohydrolytischer Abbau von K_2TiF_6 und thermochemisches Verhalten von $K_2Ti(O_2)F_4 \cdot H_2O$, Z. Anorg. Allg. Chem. 523 (1985) 213–226.
[21] M.M. Godneva, Russ. J. Inorg. Chem. [Engl. Transl.] 34 (1989) 827–830.
[22] M.S. Lee, P. Grieveson, Production of Al–Ti–B grain refining master alloys, Mater. Sci. Technol. 19 (2003) 769–772.
[23] N.E. Mahallawy, M.A. Taha, A.W. Jarfors, On the reaction between aluminium, K_2TiF_6 and KBF_4, J. Alloys Compd. 292 (1999) 221–229.
[24] R.F. Williamson, W.O.J. Boo, Lower valence fluorides of vanadium. 1. Synthesis and characterization of sodium trifluorovanadate, potassium trifluorovanadate, and rubidium trifluorovanadate, Inorg. Chem. 16 (1977) 646–648.
[25] P.Y. Chiang, T.W. Lin, J.H. Dai, B.C. Chang, K.H. Lii, Flux synthesis, crystal structure, and luminescence properties of a new europium fluoride-silicate: $K_5Eu_2FSi_4O_{13}$, Inorg. Chem. 46 (2007) 3619–3622.
[26] J. Lee, H. Shin, J. Lee, H. Chung, Q. Zhang, F. Saito, Mechanochemical syntheses of perovskite $KMIIF_3$ with cubic structure (MII = Mg, Ca, Mn, Fe, Co, Ni, and Zn), Mater. Trans. 44 (2003) 1457–1460.
[27] L.N. Demiamets, Hydrothermal synthesis of new compounds, Prog. Cryst. Growth Charact. 21 (1990) 299–355.
[28] J. Kohler, J.H. Chang, M.H. Whangbo, Bonding oxidation state of a transition metal atom encapsulated in an isolated octahedral cluster cation of main group elements: synthesis, crystal structure, and electronic structure of $Pt_2In_{14}Ga_3O_8F_{15}$ containing highly positive 18-electron complex $[PtIn_6]^{10+}$ and low-valent In^+ ions, J. Am. Chem. Soc. 127 (2005) 2277–2287.
[29] Y.P. Du, Y.W. Zhang, L.D. Sun, C.H. Yan, Luminescent monodisperse nanocrystals of lanthanide oxyfluorides synthesized from trifluoroacetate precursors in high-boiling solvents, J. Phys. Chem. C 112 (2008) 405–415.
[30] R.L. Brutchey, E.S. Yoo, D.E. Morse, Biocatalytic synthesis of a nanostructured and crystalline bimetallic perovskite-like barium oxofluorotitanate at low temperature, J. Am. Chem. Soc. 128 (2006) 10288–10294.
[31] S. Feng, R. Xu, New materials in hydrothermal synthesis, Acc. Chem. Res. 34 (2001) 239–247.
[32] C. Li, J. Yang, Z.W. Quan, P.P. Yang, J. Lin, Different microstructures of β-$NaYF_4$ fabricated by hydrothermal process: effects of pH values and fluoride sources, Chem. Mater. 19 (2007) 4933–4942.
[33] G. Corbela, E. Suardb, J. Voiron, M. Leblanca, Hydrothermal synthesis and magnetic studies of transition metal nocerites $M_3(BO_3)F_3$ (M = Fe, Co, Ni), J. Magn. Magn. Mater. 234 (2001) 423–430.
[34] T. Berrocal, J.L. Mesa, J.L. Pizarro, M.K. Urtiaga, M.I. Arriortua, T. Rojo, $Fe_2(AsO_4)F$: a new three-dimensional condensed fluoro-arsenate iron(II) compound with antiferromagnetic interactions, J. Solid State Chem. 179 (2006) 1659–1667.
[35] R. Yu, D. Wang, N. Kumada, N. Kinomura, Novel open-framework material: cerium oxyfluoride with $CeOF_2$ dodecahedron, Chem. Mater. 12 (2000) 3527–3529.
[36] D.W. Aldous, N.F. Stephens, P. Lightfoot, The role of temperature in the solvothermal synthesis of hybrid vanadium oxyfluorides, Dalton Trans. 37 (2007) 4207–4213.
[37] N.M. Laptash, Y.M. Nikolenko, L.N. Kurilenko, Fluorination of sulfide minerals with ammonium hydrogen difluoride, J. Fluorine Chem. 105 (2000) 53–58.
[38] R.A. Nyquist, R.O. Kagel, Infrared Spectra of Inorganic Compounds, Academic Press, New York/London, 1971.
[39] N.M. Laptash, I.G. Maslennikova, T.A. Kaidalova, Ammonium oxofluorotitanates, J. Fluorine Chem. 99 (1999) 133–137.
[40] K.S.W. Sing, Physisorption of nitrogen by porous materials, J. Porous Mater. 2 (1995) 5–8.
[41] S.U.M. Khan, M. Al-Shahry, W.B. Ingler Jr., Efficient photochemical water splitting by a chemically modified n-TiO_2, Science 297 (2002) 2243–2245.
[42] J.W. Tang, Z.G. Zou, J.H. Ye, Efficient photocatalytic decomposition of organic contaminants over $CaBi_2O_4$ under visible-light irradiation, Angew. Chem. Int. Ed. 43 (2004) 4463–4466.

[43] J.W. Tang, Z.G. Zou, J.H. Ye, Effects of substituting Sr^{2+} and Ba^{2+} for Ca^{2+} on the structural properties and photocatalytic behaviors of $CaIn_2O_4$, Chem. Mater. 16 (2004) 1644–1649.
[44] J. Tang, Z. Zou, J. Ye, Efficient photocatalytic decomposition of organic contaminants over $CaBi_2O_4$ under visible-light irradiation, Angew. Chem. Int. Ed. 43 (2004) 4463–4466.
[45] R. Asahi, T. Morikawa, T. Ohwaki, K. Aoki, Y. Taga, Visible-light photocatalysis in nitrogen-doped titanium oxides, Science 293 (2001) 269–271.
[46] G. Liu, L. Wang, C. Sun, X. Yan, X. Wang, Z. Chen, S.C. Smith, H. Cheng, G.Q. Lu, Band-to-band visible-light photon excitation and photoactivity induced by homogeneous nitrogen doping in layered titanates, Chem. Mater. 21 (2009) 1266–1274.
[47] K. Zhang, C. Liu, F. Huang, C. Zheng, W. Wang, Study of the electronic structure and photocatalytic activity of the BiOCl photocatalyst, Appl. Catal. B: Environ. 68 (2006) 125–129.